Rapid Local Urbanization around Most Meteorological Stations Explains the Observed Daily Asymmetric Warming Rates across China from 1985 to 2017

SHAOJING JIANG

Department of Geography and Spatial Information Techniques, Ningbo University, Ningbo, and State Key Laboratory of Earth Surface Processes and Resource Ecology, College of Global Change and Earth System Science, Beijing Normal University, Beijing, China

KAICUN WANG AND YUNA MAO

State Key Laboratory of Earth Surface Processes and Resource Ecology, College of Global Change and Earth System Science, Beijing Normal University, Beijing, China

(Manuscript received 21 February 2020, in final form 7 August 2020)

ABSTRACT: The increasing rate of the observed daily minimum temperature T_{min} has been much higher than that of the observed daily maximum temperature T_{max} during the past six decades across China. In this study, the local urbanization impact on these observed asymmetric warming rates was investigated. The latest released land-cover data with a 30-m spatial resolution and annual temporal resolution from 1985 to 2017 were used to quantify the urbanization ratios around weather stations. Although urbanized areas occupied only 2.25% of the landmass in China, the percentage of stations with an urbanization ratio over 20% increased from 22.1% to 68.2% during the period 1985–2017. Significant asymmetric warming rates at urban stations were identified, which were approximately 3 times larger compared to the average asymmetry observed at all 2454 stations in China. However, this asymmetry disappeared at rural stations. These differences are mainly due to the rapid local urbanization around most meteorological stations in China since 1985, which affected the spatial representation of observations and led to the observed asymmetry warming rates. The results reported here indicate that the observed asymmetric warming rate over China from 1985 to 2017 is an observational bias due to local urbanization around most stations rather than large-scale climate change. The results also explain the phenomenon that the observed warming rate of T_{min} remains higher than that of T_{max} after 1990 when the surface solar radiation stops decreasing in China.

KEYWORDS: Atmosphere-land interaction; Climate variability; Surface temperature; Climate records; In situ atmospheric observations; Surface observations

1. Introduction

As direct indicators of global warming, air temperatures T_a and their variations have been widely reported (Hansen and Lebedeff 1987; Easterling et al. 1997; Parker 2006). Global mean air temperature has increased by 0.86°C during the past 150 years (Hoegh-Guldberg et al. 2018), especially in China, which had reached a warming magnitude of 1.44°C during the period 1961–2013 (Sun et al. 2016). In addition, the warming trend of observed daily minimum temperature T_{min} was higher than that of observed daily maximum temperature T_{max} in China (Liu et al. 2006; Li and Yan 2009). As one of the largest developing countries in the world, China has undergone rapid urbanization since the 1978 economic reform (Huang et al. 2017; Yang et al. 2017). In 2017, the total population in China reached 1.39 billion. According to the National Bureau of Statistics of China, urban residents already made up 58.52% of the total population in China in 2017, and this number will exceed 80% by 2050.

Existing studies have investigated the factors contributing to the asymmetric warming rates between T_{min} and T_{max} in China (Peng et al. 2013; Bian and Ren 2017). Some studies identified a reduction in solar radiation from the 1950s to the 1980s in China (Gilgen et al. 1998; K. Wang et al. 2015), which slows down the warming rate of T_{max} and partly explains the spatial pattern of warming rate in China from 1960 to 2003 (Du et al. 2017). However, the warming rate of T_{min} remains higher than that of T_{max} after 1990 (Li et al. 2010) when the surface solar radiation stops decreasing in China (He et al. 2018).

Another possible factor is the local urbanization impact on air temperatures (Li et al. 2010; Yang et al. 2011; Sun et al. 2016), especially the urban heat island (UHI) effect, which refers to the phenomenon that urban areas being warmer than surrounding rural areas and has been the focus of numerous studies (Oke 1973; Grimmond 2007; Stewart and Oke 2012; Li et al. 2014; Kaloustian and Diab 2015). The UHI indicates climate change at a local scale and it is generated during the urbanization process. The contrast in land cover between urban and rural areas alters surface net radiation and its partition into latent and sensible heat fluxes (Oke 1982; Miao et al. 2012; Xu et al. 2018), which leads to a weak daytime UHI and a strong nighttime UHI in most inland cities with the exception of some cities in desert areas (Lazzarini et al. 2013; Founda and Santamouris 2017).

Many researchers have noticed a difference between the observed T_{min} and T_{max} warming trends, and attributed it to the UHI effect, which can lead to significantly higher nighttime air temperatures in urban areas than in rural areas in most regions (Zhao et al. 2014; K. Wang et al. 2017). It is essential to classify urban and rural stations in UHI studies. Population,

Corresponding author: Kaicun Wang, kcwang@bnu.edu.cn

DOI: 10.1175/JCLI-D-20-0118.1

gross domestic product (GDP), and satellite night light data were used as the standards for selecting urban stations in previous studies (Hua et al. 2008). Nevertheless, regional population density and GDP are not directly correlated with the microclimate around meteorological stations, and satellite night light data were not available before 1992 (Liu et al. 2012). As a result, conclusions of such studies are not always consistent (Hua et al. 2008; Yang et al. 2011; Wen et al. 2019).

These inconsistent results are obtained partly due to the selection of different stations. In this study, urban stations were first taken as a representative group of stations to cohere with the inconsistent observations of the daily asymmetric warming rates and solar radiation change after 1990 (Li et al. 2010). Moreover, warming rates at rural stations and all stations were compared with those at urban stations. The land-cover change data could well describe the environment changes around weather stations and is directly related to the local impact of the urbanization process on the observed warming rates (Vose et al. 2004; Kaloustian and Diab 2015; Akbari et al. 2015). Such information has long been regarded as a reference to classify urban and rural areas (Stewart and Oke 2012; Singh et al. 2017; Li et al. 2019).

This study aims to explain the observed daily asymmetric warming rates in China and improve the assessment of the local urbanization impact on them based on the latest released land-cover dataset at annual temporal resolution and 30-m spatial resolution. This dataset could quantity the urbanization rate and help to classify urban and rural stations more accurately and reliably. Combined with the collection of daily T_a observations, the observed asymmetric warming rates between T_{min} and T_{max} at urban stations, rural stations, and all stations could be compared. In addition, this analysis permits us to assess local urbanization impacts on the observed warming rates at annual time scales. On average, local urbanization ratios account for 75% (for T_{max}), 98% (for T_{min}), and 97% (for T_{mean}) of the annual anomaly of urban–rural T_a differences. This study is the first to identify that the observed asymmetric warming rates over China from 1985 to 2017 is an observational bias due to local urbanization around most stations rather than large-scale climate change.

2. Data and methods

Ground-based daily meteorological observations of T_{mean}, T_{max}, and T_{min} collected at 2454 stations in China from 1985 to 2017 (Fig. 1) were obtained from the China Meteorological Administration. The T_{mean} represents the average of four regularly timed observations collected at 0200, 0800, 1400, and 2000 Beijing time. The dataset had already passed quality control standards before it was obtained from the China Meteorological Administration. The quality control procedures include checks of plausible values, time consistency, internal consistency, historical values, and spatial distribution (Dou et al. 2008). After the quality control process, the questionable rate of the daily air temperature dataset was less than 0.01% according to the evaluation report of the China Meteorological Administration, and its overall data missing rate was less than 0.05%. Because this study focuses on the gradual urbanization impact, only the longest continuous record without relocations was used for each station.

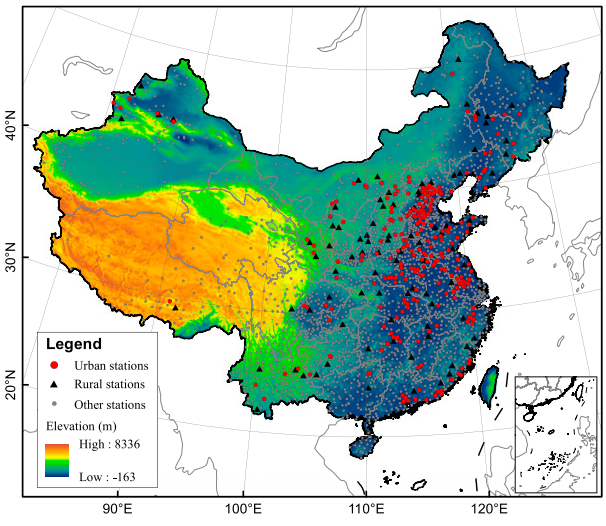

FIG. 1. The elevation of the study area and locations of 242 urban stations, 87 rural stations, and 2125 other stations.

The long-term (1985–2017), high-resolution (30 m) land-cover datasets in China were produced by Gong et al. (2019a,b). There are two kinds of land-cover types, which are urban surfaces and nonurban surfaces. Urban surfaces are impervious surfaces, which include building roofs, concrete pavement, driveways, and parking lots. Other nonimpervious surfaces are regarded as nonurban surfaces, including grasslands, forests, croplands, shrub, wetland, bare land, tundra, and water. Landsat images obtained during growing seasons were the primary source to map this dataset. An improved supervised classification method using an inventory-based training set was applied in the automatic impervious surface mapping framework (Li et al. 2015; Li and Gong 2016). Although there is some uncertainty in time and space in this product because of the confusion between impervious surfaces and barren (Li et al. 2015), the overall accuracy of this dataset has reached more than 90%. Apart from impervious surfaces, built-up area density, building height, and other factors may also contribute to urban warming, which need to be further analyzed when these data become available.

In this study, the urbanization ratio, which was defined as the percentage of impervious surfaces within a circular area of 10 or 100 km^2 around the station, was used to select urban stations and rural stations. Similar classification methods have been applied in previous researches (Ren and Ren 2011; Hausfather et al. 2013; Chrysanthou et al. 2014; Li et al. 2017; Wen et al. 2019). According to the National Bureau of Statistics of China, there are ~600 cities in China, and 99% of them cover an area of more than 100 km^2 while more than 96% of them have a built-up area of more than 10 km^2 in 2017. Therefore, 10 and 100 km^2 are considered to avoid the selection of stations in urban parks and star towns in rural areas. The urbanization ratio was calculated once a year, and each station had a 33-yr series of urbanization ratio data. Urban stations were selected based on Eq. (1):

$$\begin{cases} R_{\max} \geq 50\% \\ \text{RATE} \geq 1\%\ \text{yr}^{-1} \end{cases}, \quad (1)$$

where $R_{\max}$ is the maximal urbanization ratio at the station during the period of the longest continuous record, and RATE is the increasing rate of urbanization ratio during the period of the longest continuous record. The urbanization ratio within 10 and 100 km^2 were both considered, only when they both meet the requirement of Eq. (1), the station was classified as an urban station.

After classifying urban stations, rural stations were selected from the remaining stations to pair with each urban station. The location and size for rural stations are consistent with the requirement of the World Meteorological Organization guide because there is less urbanization. A rural station is always set up in an open grassland far away from tall buildings with a size ranging from 10 m × 7 m to 25 m × 25 m. The selection of rural stations is based on the following considerations: 1) The maximal urbanization ratios within 10 and 100 km^2 were both lower than 20% during the period of the continuous record, and 2) the distance between the rural station and the paired urban station was more than 20 km and less than 150 km. Since there were several qualified rural stations for some urban stations, only the rural station with the longest continuous record and the shortest distance from the urban station was selected. In addition, any urban–rural station pair with a coincident time duration of less than 10 years was excluded. (The time series of mean urbanization ratios at selected urban stations and rural stations are shown in Fig. 4.)

Different classification methods had been applied in previous studies. For example, Stewart and Oke (2012) built a classification system based on detailed land-cover data to classify urban and rural stations. Muller et al. (2013) proposed a network-scale classification scheme based on area size, the spatial density, and the representativeness of stations within the network. Compared to these studies, the classification method for urban and rural stations in this study is a bit different because this study is based on conventional meteorological observations rather than high-resolution urban networks, and the detailed information of land-cover types is lacking.

The monthly T_a anomaly was calculated as the difference between the monthly T_a and its corresponding monthly mean climate state. The monthly mean climate state used in this study at each station was the monthly average T_a during the period 1985–2014, because 30 years is generally regarded as the time duration to calculate a mean climate state (Tang and Zhai 2005; Arguez and Vose 2011; Lin and Zhang 2015) that was recommended by the World Meteorological Organization (WMO 2011). To reduce the heterogeneity, stations that were close to the desert or rivers were not selected as urban or rural stations. The urban–rural T_a anomaly difference was defined as the T_a anomaly difference between urban stations and their paired rural stations. Ultimately, 242 urban stations and 87 rural stations were selected to evaluate the urbanization impact on T_a, which means that some urban stations share a rural station, as shown in Fig. 1. The other stations (Fig. 1) were not considered in the evaluation of the urbanization impact on T_a at urban stations but were considered in the evaluation of national average warming trends and national average urbanization impacts on T_a.

The urbanization effect (UE) at urban stations was the trend of the mean urban–rural T_a anomaly difference (ΔT), which was calculated using Eq. (2):

$$\Delta T = \frac{\sum_{i=1}^{n} (\text{UT}_i - \text{RT}_i)}{n}, \quad (2)$$

where UT_i is the T_a anomaly at the urban station i, RT_i is the T_a anomaly at the paired rural station, and n is the number of total urban–rural station pairs ($n = 242$). The ΔT is the simple average of the T_a anomaly difference at 242 urban–rural pair stations. The simple average is calculated rather than the area-weighted average because most station pairs are located in Eastern China (Fig. 1). The UE is the trend of ΔT, which was obtained from the linear regression Eq. (3):

$$\begin{cases} \Delta T_i = b + a \times y_i \quad (i = 1, 2, 3, \ldots n_y) \\ UE = a \times 10 \end{cases}, \quad (3)$$

where ΔT_i is the mean urban–rural T_a anomaly difference at year i, y_i is the observation year, n_y is the total number of years ($n_y = 33$), a is the regression coefficient, and b is the constant. The unit of UE is degrees Celsius per decade (°C decade^{-1}).

The urbanization contribution (UC) at urban stations was calculated using Eq. (4):

$$\text{UC} = \left(\frac{\text{UE}}{\text{UT}}\right) \times 100\%, \quad (4)$$

where UT is the trend of the mean urban T_a anomaly at 242 urban stations, and UE is obtained from Eq. (3). Similar computing methods to quantify the urbanization impact on T_a, for example, the definitions of UE and UC have been put forward and applied in previous studies (Wang et al. 2013; Sun et al. 2016; Bian and Ren 2017).

3. Results and discussion

a. Rapid local urbanization around weather stations

Figure 2a shows the distribution of impervious surfaces in China in 2017, and most impervious surfaces were distributed in Eastern China. The total impervious surfaces only occupied 2.25% of the landmasses in China in 2017 (Fig. 2b). All 2454 weather stations were unevenly distributed, most of which were located in central east China (Fig. 1). The percentage of stations with an urbanization ratio within 10 km^2 larger than 20% was 68.2% in 2017, only 31.8% of the stations had an urbanization ratio under 20% in 2017 (Fig. 2c).

Figure 3 shows the interdecadal variation in urbanization ratios around all 2454 weather stations since 1985. Among all of the stations, 77.9% of them had an urbanization ratio ranging from 0% to 20% in 1985, but the number of such stations decreased to 31.8% in 2017. Meanwhile, the number of stations with an urbanization ratio over 20% has increased rapidly from 22.1% in 1985 to 68.2% in 2017, which implies the immediate areas around the stations have become more

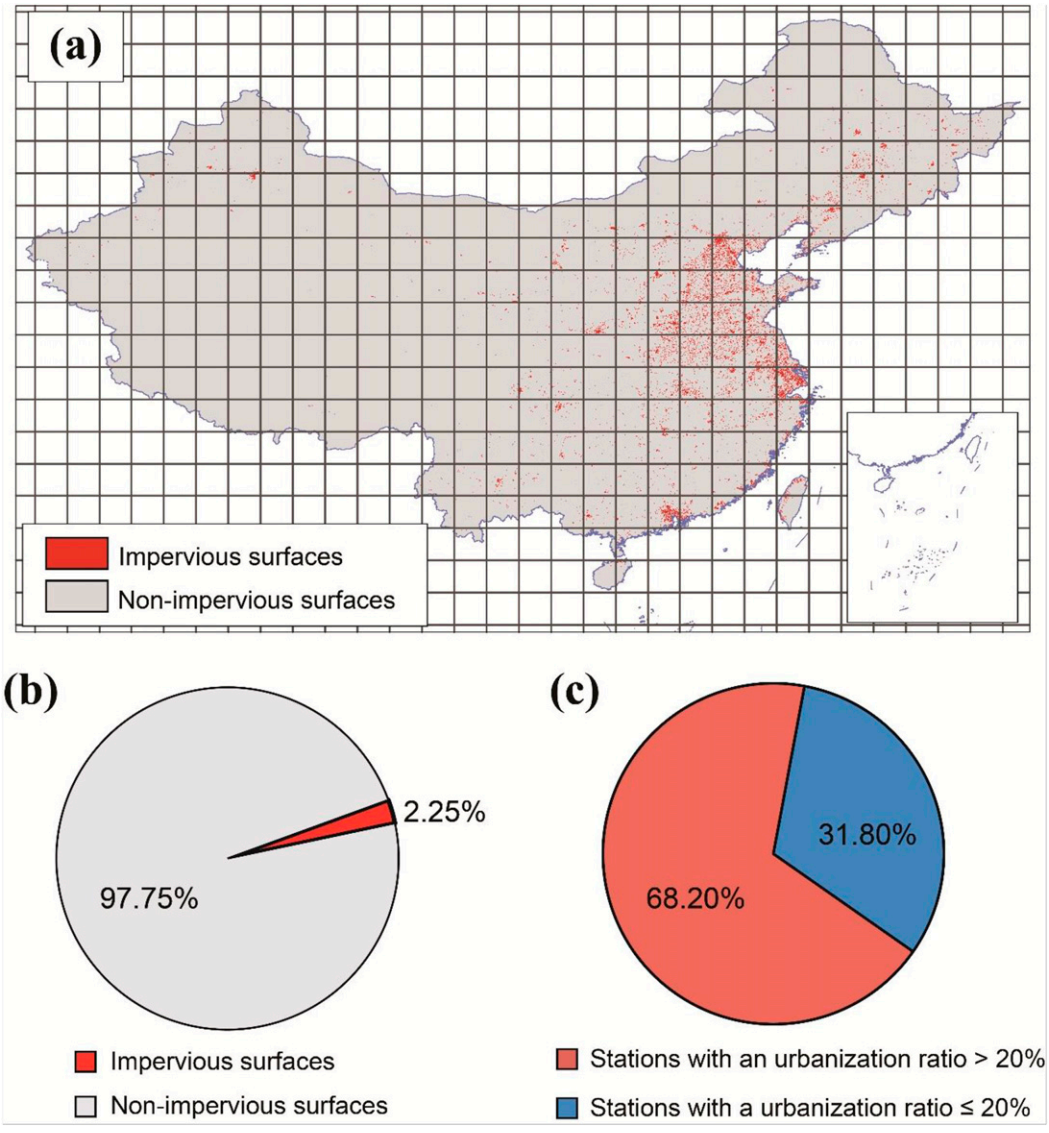

FIG. 2. The (a) distribution and (b) percentages of impervious surfaces and nonimpervious surfaces in China in 2017, and (c) the percentages of stations with different urbanization ratios within 10 km^2 in 2017.

urbanized. The urbanization ratio difference was obvious between urban and rural stations (Fig. 4), which showed an increasing rate in the urbanization ratio within 10 km^2 of 16.75% and 0.84% $decade^{-1}$, respectively. A similar difference was observed for the urbanization ratio within 100 km^2 (Fig. 4b).

b. Observed asymmetric warming rates between T_{min} and T_{max}

The national average warming rates in China were calculated across all 2454 stations during warm seasons (May–October), cold seasons (November–April), and the whole year, as shown in Fig. 5 and Table 1. Significant warming trends were observed for T_{max}, T_{min}, T_{mean}, and $T_{(max+min)/2}$ (the average of T_{max} and T_{min}), with annual averages of 0.356°, 0.421°, 0.347°, and 0.388°C $decade^{-1}$, respectively. The warming rates during cold seasons were slightly (0.015–0.044°C $decade^{-1}$) higher than those during warm seasons. $T_{(max+min)/2}$ is also investigated for comparison because it has been widely used in the international climate change study community (Wang 2014). The annual warming trend of T_{mean} (0.347°C $decade^{-1}$) in China was a bit weaker than that of $T_{(max+min)/2}$ (0.388°C $decade^{-1}$), and they were both stronger than those in previous studies, for example, 0.23°C $decade^{-1}$ for T_{mean} during the period 1961–2015 (Wen et al. 2019) and 0.305°C $decade^{-1}$ for $T_{(max+min)/2}$ during the period 1961–2008 (Ren and Zhou 2014) in China. This difference is because different study period (the period after the 1978 economic reform) was analyzed in this study. The warming rates of $T_{(max+min)/2}$ are slightly higher than those of T_{mean} at both

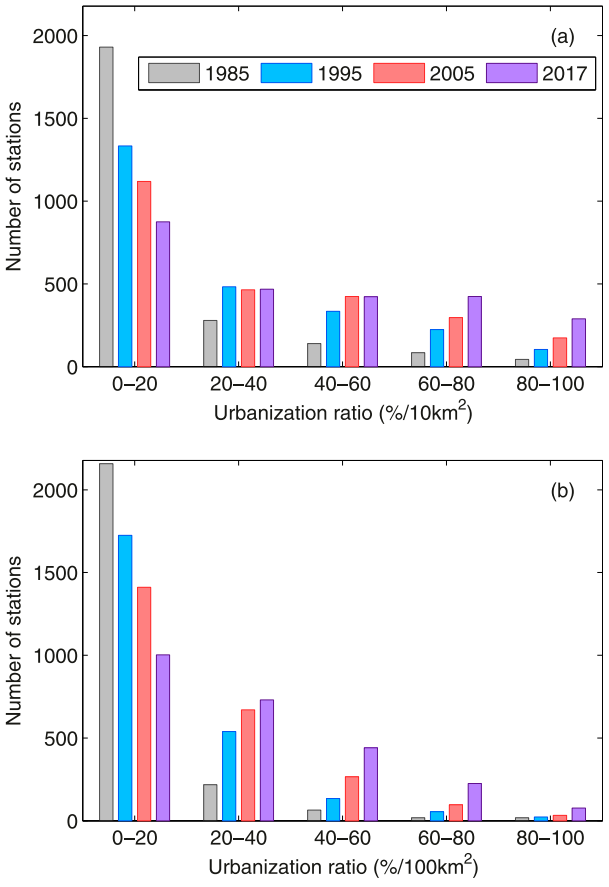

FIG. 3. Numbers of stations with different urbanization ratios derived from circular areas of (a) 10 km^2 and (b) 100 km^2 in 1985, 1995, 2005, and 2017. All panels share the same legend as in (a).

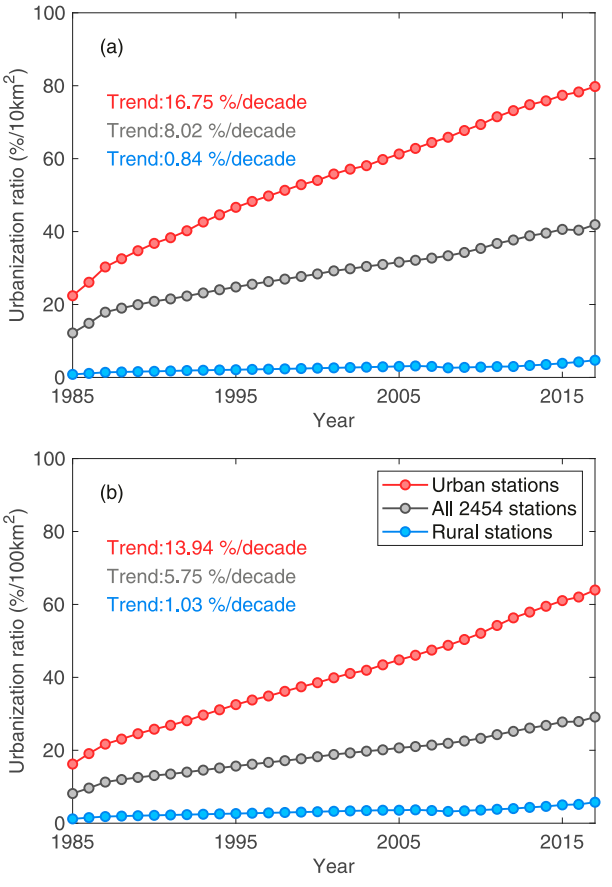

FIG. 4. Time series of mean urbanization ratios at urban stations, rural stations, and all 2454 stations derived from circular areas of (a) 10 km^2 and (b) 100 km^2. All panels share the same legend as in (b).

urban and rural stations. Compared to T_{mean}, $T_{(max+min)/2}$ only samples T_a twice a day. Studies had identified that $T_{(max+min)/2}$ would overestimate the average warming rates in most areas of China (Liu et al. 2019). This difference may be due to a rightward skew in the daily temperature curve, which is closer to T_{min} (Bernhardt et al. 2018; Bernhardt and Carleton 2019) since air temperature increases faster after sunrise than it decreases after sunset (K. Wang et al. 2017).

In addition, the national average warming trend of T_{min} was 0.065°C decade^{-1} stronger than that of T_{max} throughout the whole year, and this asymmetry during cold seasons (0.054°C decade^{-1}) is lower than that during warm seasons (0.078°C decade^{-1}). This result was consistent with that of Li et al. (2019), that is, the asymmetric difference in the warming rates between T_{min} and T_{max} was 0.085°C decade^{-1} across China during the period 1977–2014, but was smaller than the asymmetry (0.153°C decade^{-1}) in China during the period 1961–2008 (Ren and Zhou 2014). Obvious asymmetric warming rates have also been observed at a regional scale other than those national average values, especially in megacities. For example, the asymmetry between T_{min} and T_{max} was 0.47°C decade^{-1} in Shijiazhuang city from 1960 to 2012 (Bian and Ren 2017) and 0.328°C decade^{-1} in Beijing city from 1978 to 2008 (Wang et al. 2013).

The regional difference in the asymmetric warming rates drove us to compare the warming effects between urban and rural areas: 242 stations with rapid urbanization around them were regarded as urban stations; 87 stations with very low urbanization around them were selected as rural stations and paired with the urban stations. Thus, the warming rates at urban and rural stations were analyzed separately (Figs. 6–8), which helped clarify the asymmetric warming rates between T_{min} and T_{max}. The result revealed a significant warming trend in T_a at both urban and rural stations during warm seasons (Fig. 7), cold seasons (Fig. 8), and the whole year (Fig. 6).

The asymmetry between T_{min} and T_{max} at urban stations (0.197°C decade^{-1}) was approximately 3 times larger than that derived at all 2454 stations (0.065°C decade^{-1}) throughout the year. Moreover, this asymmetry also occurred during warm seasons (Figs. 7a,b and Table 1) and cold seasons (Figs. 8a,b), but was greater during warm seasons (0.204°C decade^{-1}) than that of cold seasons (0.191°C decade^{-1}). However, this asymmetry nearly disappeared at rural stations (0.005°C decade^{-1}). Interestingly, the annual warming trends of T_{max} at urban and

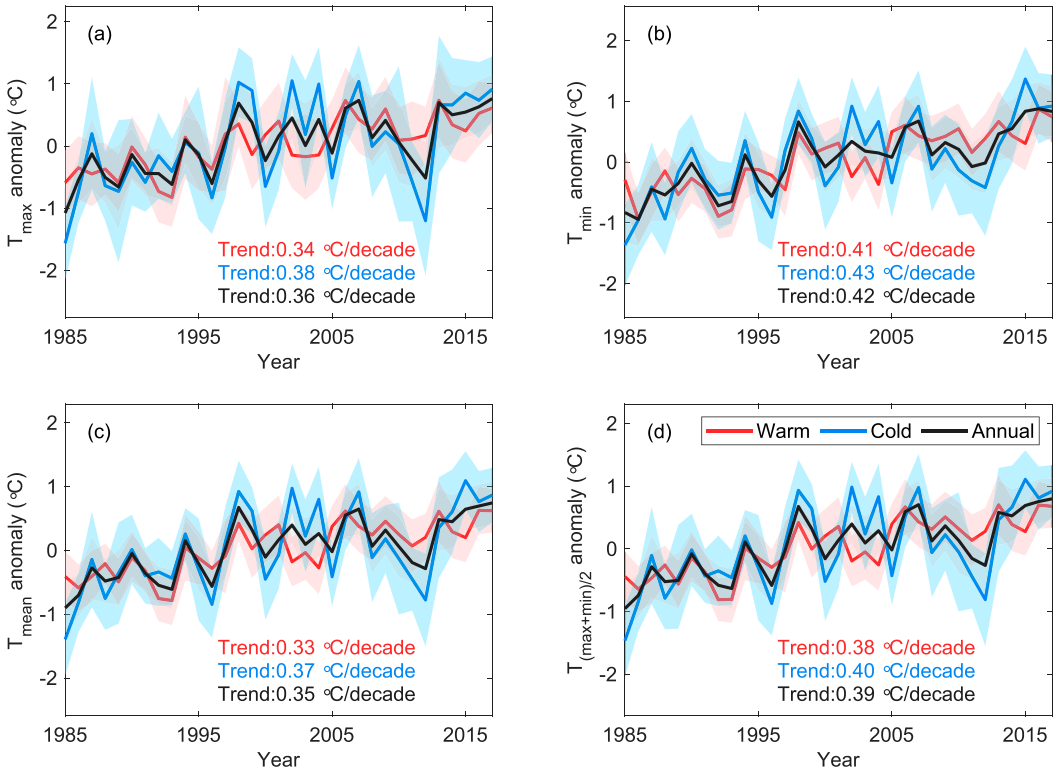

FIG. 5. Time series of (a) T_{max}, (b) T_{min}, (c) T_{mean}, and (d) $T_{(max+min)/2}$ anomalies averaged from all 2454 stations during warm seasons (May–October), cold seasons (November–April), and the whole year. The shading indicates the standard deviation of T_a anomalies at all 2454 stations during warm seasons (pink), cold seasons (light blue), and the whole year (gray), with the overlap shown in light gray. All panels share the same legend as in (d).

rural stations (0.378° and 0.358°C decade^{-1}, respectively) were very similar, whereas for T_{min}, the annual warming trend at urban stations (0.575°C decade^{-1}) was much stronger than that at rural stations (0.353°C decade^{-1}). These differences drove us to explore more on the local urbanization impact on this asymmetry.

c. *Local urbanization impacts on the observed asymmetry at urban stations*

The local urbanization impact on T_a anomaly at 242 urban–rural station pairs during the period 1985–2017 is shown in Figs. 9 and 10 . Figure 9 shows the number of station pairs with different trends in urban–rural T_a anomaly differences during

TABLE 1. The warming trends (°C decade^{-1}) in T_{max}, T_{min}, T_{mean}, and $T_{(max+min)/2}$ anomalies averaged from all 2454 stations, urban stations, and rural stations, respectively. Warm seasons represent the period from May to October, and cold seasons represent the period from November to April. The $T_{(max+min)/2}$ was averaged from T_{max} and T_{min}. A two-tailed t test is employed to test the significance of the warming trend. Asterisks (*) indicate significance at the $p = 0.01$ confidence level.

Stations	T_a anomaly	Trend (°C decade^{-1})		
		Warm seasons	Cold seasons	The whole year
All 2454 stations	T_{max}	0.336*	0.375*	0.356*
	T_{min}	0.414*	0.429*	0.421*
	T_{mean}	0.325*	0.369*	0.347*
	$T_{(max+min)/2}$	0.375*	0.402*	0.388*
Urban stations	T_{max}	0.354*	0.401*	0.378*
	T_{min}	0.558*	0.592*	0.575*
	T_{mean}	0.417*	0.474*	0.445*
	$T_{(max+min)/2}$	0.456*	0.497*	0.476*
Rural stations	T_{max}	0.335*	0.382*	0.358*
	T_{min}	0.359*	0.348*	0.353*
	T_{mean}	0.282*	0.328*	0.305*
	$T_{(max+min)/2}$	0.347*	0.365*	0.356*

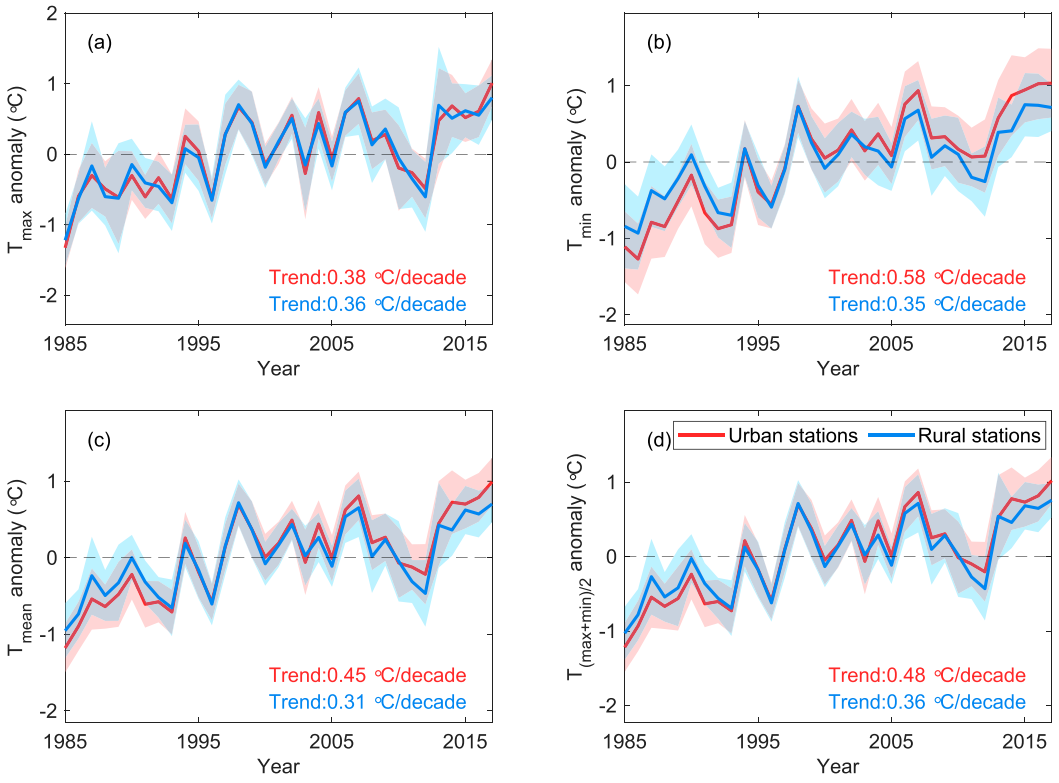

FIG. 6. Time series of (a) T_{max}, (b) T_{min}, (c) T_{mean}, and (d) $T_{(max+min)/2}$ anomalies at urban and rural stations during the whole year. The shading indicates the standard deviations of T_a anomalies at all urban stations (pink) or at all rural stations (light blue), i.e., the interstation deviation of T_a anomalies each year, with the overlap shown in light gray. All panels share the same legend as in (d).

warm seasons, cold seasons, and the whole year. More than 82.2% of the station pairs exhibit an increasing trend in annual T_{mean} anomaly differences during the study period. In contrast, the percentage of station pairs with positive anomaly difference trends derived for T_{max} (68.6%) was not as large as those derived for T_{min} (79.8%) and $T_{(max+min)/2}$ (79.3%).

Previous studies have shown that urbanization can be well characterized by the percentages of different land-cover types (Zhou et al. 2004; K. Wang et al. 2017). Therefore, the correlation between urban–rural T_a anomaly differences and urban–rural urbanization ratio differences was also analyzed to explore the urbanization impact on air temperatures (Fig. 10). A significant correlation relationship between T_a anomaly difference and urban–rural urbanization ratio difference was observed at most stations. More than 84.7% of the station pairs exhibited a positive correlation between the urban–rural T_{mean} anomaly differences and the urban–rural urbanization ratio differences (Fig. 10), while for T_{min} and T_{max}, the numbers were lower, that is, 69.0% and 66.9%, respectively. T_{mean} was averaged from four regularly timed observations (0200, 0800, 1400, and 2000 Beijing local time) (Jiang and Wang 2018), whereas the time occurrences of T_{max} and T_{min} varied (Li et al. 2016). Therefore, T_{mean} did not show the strongest correlation with urbanization ratio compared to T_{max} and T_{min} but tends to exhibit more consistent correlations (i.e., positive correlations) with the urbanization ratio.

The negative results in Figs. 9 and 10 may mainly be related to the locations and surroundings of the urban–rural station pairs. Several coastal urban stations in Eastern China are closer to the ocean than the paired rural stations. Although several coastal urban stations have gone through rapid urbanization, they show a lower warming rate than their paired rural stations due to the sea–land thermal difference (Sutton et al. 2007; Torres-Alavez et al. 2014). Previous studies had identified negative UHIs in coastal cities when inland rural stations were regarded as the rural reference (Jiang et al. 2019). Another factor for the negative results is elevation. Several rural stations are located in mountain regions with a higher elevation than their paired urban stations, whereas the warming trends in high elevation regions tend to be higher than regions with lower elevations (You et al. 2008; Pepin et al. 2015; L. Yan et al. 2016). Additionally, higher air pollution in urban areas reduces the amount of solar radiation that reaches the urban canopy floor during the daytime, which may decrease T_{max} and contribute to negative urban–rural T_{max} difference (Easterling et al. 1997; Zheng et al. 2018).

The average urbanization impact on T_a anomaly at 242 urban–rural station pairs during the period 1985–2017 is shown

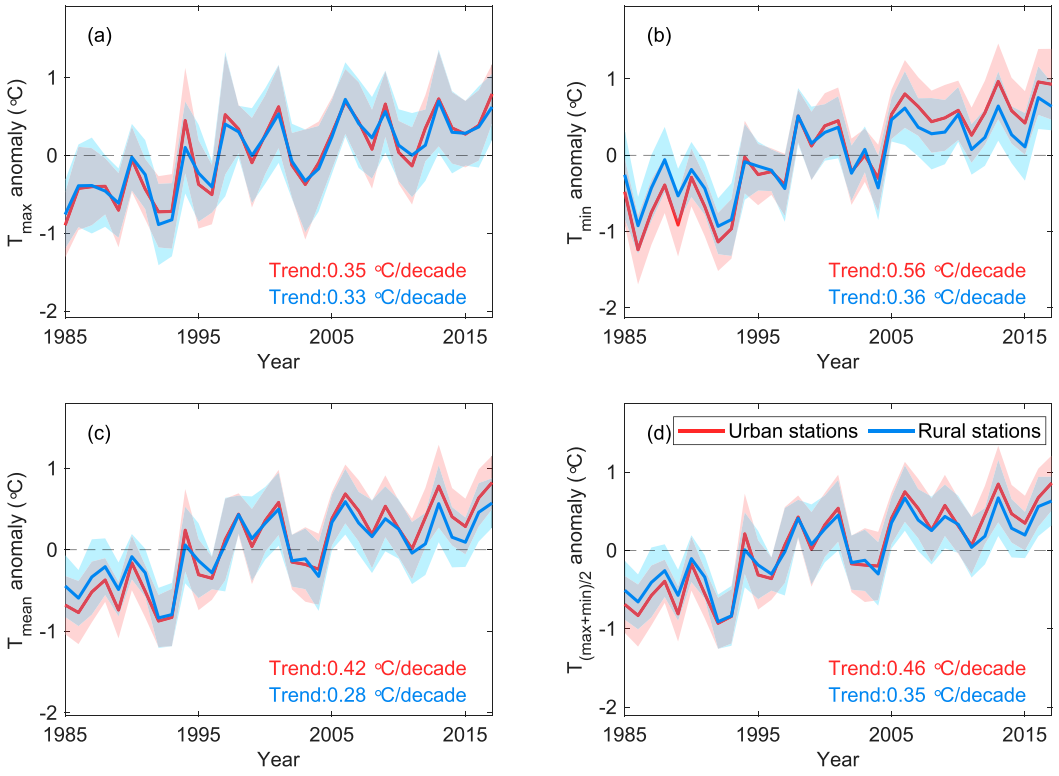

FIG. 7. As in Fig. 6, but derived during warm seasons (May–October) instead of the whole year.

in Fig. 11 and Table 2. It can be seen that T_a anomaly differences were negative from 1985 to 1995 and were mainly positive from 1996 to 2017. The negative results may be related to the changes in rural land-cover types and low urbanization ratios (<50%) before 1995 (Fig. 4). The T_{max}, T_{min}, T_{mean}, and $T_{(max+min)/2}$ anomaly differences all show significant increasing trends during the period 1985–2017, with the strongest UE on T_{min} (annual: 0.243°C decade^{-1}) and the weakest UE on T_{max} (annual: 0.050°C decade^{-1}). The annual changes in T_{mean} and $T_{(max+min)/2}$ anomaly differences were very similar, with increasing trends of 0.163°C decade^{-1} and 0.146°C decade^{-1}. Local urbanization impacts on T_a were slightly stronger during cold seasons than during warm seasons except for T_{max}. Apart from the UE, the UC to T_a at urban stations was also shown in Table 2. It can be seen that the UC to the annual T_{min} reached 42.2% at urban stations, while for the annual T_{max}, the UC was 13.2%. The UC to the annual T_{mean} (36.7%) was slightly stronger than that to annual $T_{(max+min)/2}$ (30.7%). This difference is related to the difference in sampling times between $T_{(max+min)/2}$ and T_{mean}.

Considering the unequal numbers of urban and rural stations, the local urbanization impact on T_a using only 87 single urban–rural station pairs was also compared (Table 3). The nearest urban station was selected to couple with each rural station. Significant increasing trends in T_a anomaly differences during the period 1985–2017 were also observed. The annual UE on T_{max}, T_{min}, T_{mean}, and $T_{(max+min)/2}$ anomaly differences were 0.043°, 0.214°, 0.146°, and 0.129°C decade^{-1}, respectively. The annual UC to T_{max}, T_{min}, T_{mean}, and $T_{(max+min)/2}$ were 11.0%, 37.7%, 32.6%, and 26.7%, respectively. The UE on and UC to T_a derived from 87 single urban–rural station pairs were slightly lower than those derived from 242 urban–rural station pairs. This difference may be related to the urbanization ratio. The increasing rate in urbanization ratio at 87 stations within 10 km^2 is 16.39% decade^{-1}, which is slightly lower than that at 242 stations (16.75% decade^{-1}). This difference may contribute to a slower warming rate at 87 stations and lead to lower UE and UC.

The result was slightly different from other studies, which may relate to selections of different study periods, datasets, and station classification methods. The period after the economic reform (Huang et al. 2017; Yang et al. 2017) was analyzed and stations with rapid urbanization surroundings were classified as urban stations. For the study by Ren and Zhou (2014), the UE on (UC to) warming trends of T_{max}, T_{min}, and $T_{(max+min)/2}$ across China during the period 1961–2008 were 0.023°C decade^{-1} (10.1%), 0.070°C decade^{-1} (18.4%), and 0.047°C decade^{-1} (15.4%), respectively. J. Wang et al. (2017) concluded that the urbanization explained 9% of the warming trend in T_{min} in Eastern China during the period 1980–2009. Sun et al. (2019) indicated that urbanization explained one-third of the observed warming in nighttime extremes from 1958 to 2012 across Eastern China. Bian and Ren (2019) concluded that the UE on T_{min}, T_{mean} and diurnal temperature (DTR) during the period 1960–2012 were 0.25°, 0.47°, and −0.50°C decade^{-1}, respectively.

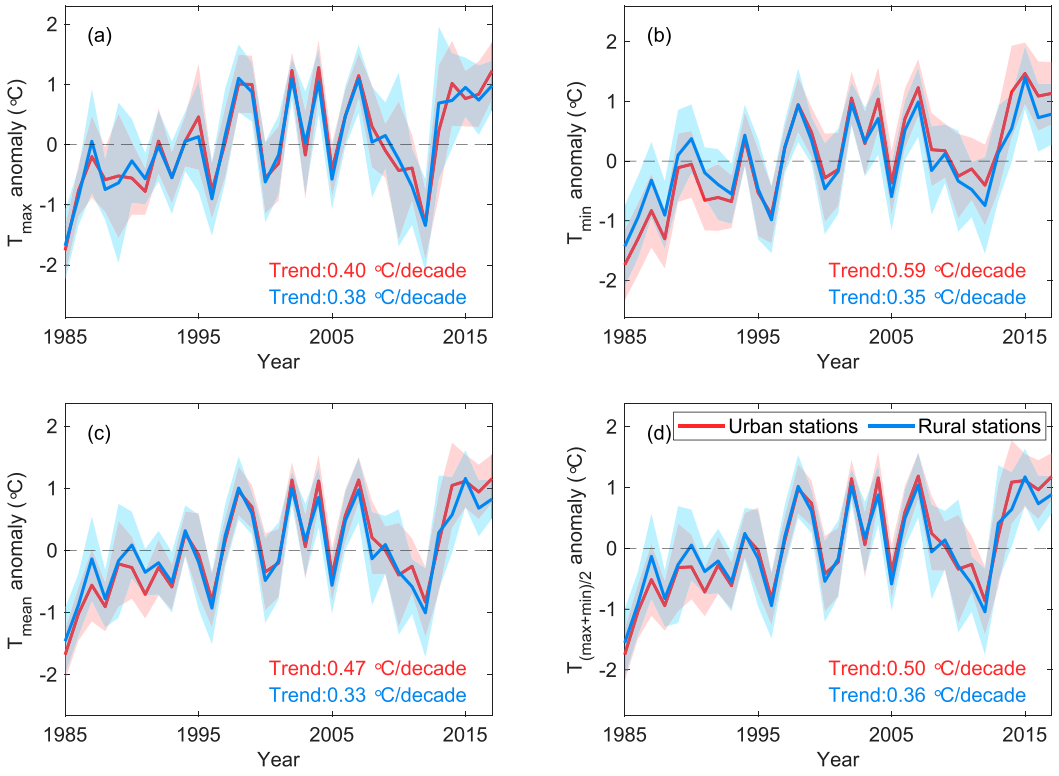

FIG. 8. As in Fig. 6, but derived during cold seasons (November–April) instead of the whole year.

d. Local urbanization impacts on the observed asymmetry in national average warming rates

To better quantify the local urbanization impact on the observed T_a across China, the national average UE and UC at all 2454 stations were also calculated in Table 4. Figure 12 presents scatterplots of mean urban–rural urbanization ratio differences at 242 urban–rural station pairs as a function of annual urban–rural T_a anomaly differences. It can be seen that urbanization ratio differences are closely related to T_a anomaly differences. The square of their correlation coefficients (r^2) at urban stations reached 75% (for T_{max}), 98% (for T_{min}), and 97% (for T_{mean}), respectively. Generally, urban impervious surfaces have larger heat capacity than natural surfaces. Therefore, more solar radiation energy is absorbed and stored in urban materials during the daytime. These energies are then released by urban material at night and weaken the urban cooling efficiency (Oke 1976, 1982; Rinner and Hussain 2011). Therefore, nighttime UHIs are stronger than daytime UHIs in most inland cities (Oke 1982; Jiang et al. 2019), which leads to a stronger impact on T_{min} than T_{max} at urban stations. The thermal storage at rural stations is much lower due to a low urbanization ratio. This difference contributes to the ''nearly disappeared'' observed asymmetric warming rates between T_{min} and T_{max} at rural stations (Wang et al. 2017).

Since there was no ideal rural reference existed to pair every weather station, a polynomial fit based on the significant positive relationship between urbanization ratio differences and T_a anomaly differences (Fig. 12) was applied. This linear regression relationship at urban stations was shown in Eq. (5):

$$\Delta T_u = b + a \times \Delta R_u, \tag{5}$$

where ΔT_u is the mean urban–rural T_a anomaly difference, ΔR_u is the mean urban–rural urbanization ratio difference, a is the regression coefficient, and b is the constant. It is assumed that the theoretic national average T_a anomaly difference (ΔT_{all}) and the ideal national average urbanization ratio difference (ΔR_{all}) have the same relationship as that in Eq. (5). Therefore, the national average UE and UC were calculated using Eq. (6):

$$\Delta T_{all} = b + a \times \Delta R_{al}, \tag{6}$$

where a and b are obtained from Eq. (5). Ideally, the urbanization ratio of a rural reference is zero; therefore, the mean urbanization ratio at all 2454 stations (gray lines in Fig. 4) can be regarded as ΔR_{all}. The urbanization ratio within 10 km^2 around the station was used in Eqs. (5) and (6). Thus, ΔT_{all} can be obtained from Eq. (6). Afterward, the national average UE and UC can be calculated using Eqs. (3) and (4), except that ΔT_i and UT are replaced with ΔT_{all} and T_{all} (the national average T_a anomaly at all 2454 stations), respectively.

The national annual average UE values on T_{max}, T_{min}, T_{mean}, and $T_{(max+min)/2}$ anomaly differences were 0.026°, 0.127°, 0.085°, and 0.076°C decade^{-1} (Table 4), respectively. The national annual average UC values to T_{max}, T_{min}, T_{mean}, and

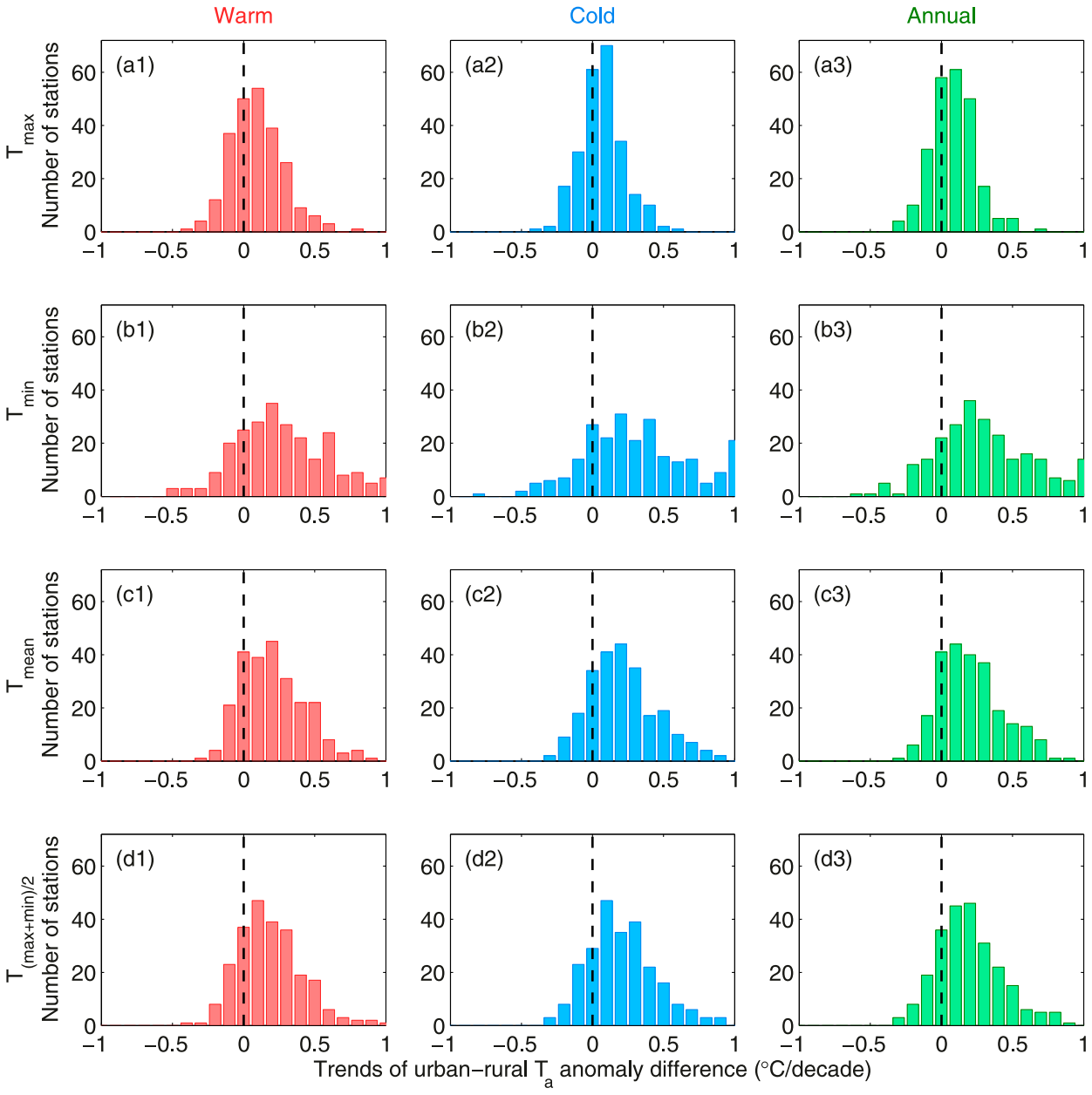

FIG. 9. Numbers of stations with different trends in urban–rural T_a anomaly differences derived for (a1)–(a3) T_{max}, (b1)–(b3) T_{min}, (c1)–(c3) T_{mean}, and (d1)–(d3) $T_{(max+min)/2}$ during warm seasons (May–October), cold seasons (November–April), and the whole year.

$T_{(max+min)/2}$ anomaly differences were 7.2%, 30.2%, 24.4%, and 19.7% (Table 4), respectively. The national average UE on T_{min} is also much stronger (0.101°C decade^{-1}) than that on T_{max}, and this difference is more obvious during cold seasons (0.120°C decade^{-1}) than that during warm seasons (0.083°C decade^{-1}). The UC to annual T_a values derived from all 2454 stations were 6.0%–12.3% lower than those derived from 242 urban–rural station pairs. This difference could be attributed to the lower urbanization ratio averaged from all 2454 stations.

The superiority of the method applied here is that high-resolution land-cover data were used instead of other factors, which are mostly not directly related to the observational environment. Nevertheless, previous studies have also analyzed the urbanization impacts on national warming trends in China based on data collected at a large number of meteorological stations, which were not as many as those used in this study. For example, Tysa et al. (2019) collected data from 2286 stations and concluded that the UC to T_{mean} was 17.6% during the period 1980–2015. Zhang et al. (2010) collected data from 752

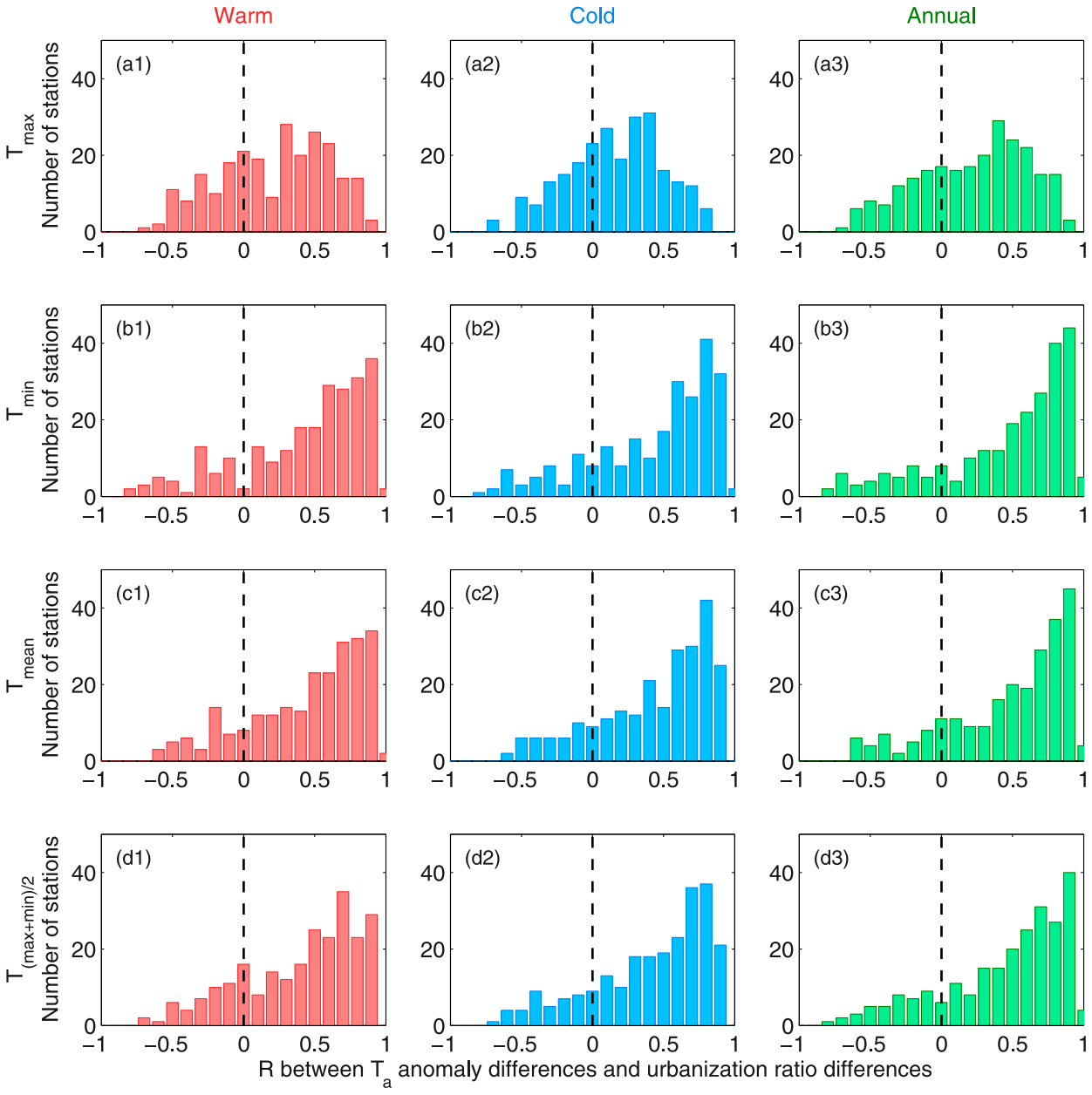

FIG. 10. The number of stations with different correlation coefficients (R) between urban–rural T_a anomaly differences and urban–rural urbanization ratio differences during warm seasons, cold seasons, and the whole year. The urban–rural T_a anomaly differences are derived from (a1)–(a3) T_{max}, (b1)–(b3) T_{mean}, (c1)–(c3) $T_{(max+min)/2}$, and (d1)–(d3) T_{min} anomalies. The urbanization ratio in a circular area of 10 km^2 was used.

stations and concluded that the UC to the warming trend of T_{mean} was 27.33% (0.076°C $decade^{-1}$) during the period 1961–2004. Shi et al. (2019) used data collected from 975 stations and concluded that the UE on T_{mean} was 0.034° ± 0.005°C $decade^{-1}$. Wen et al. (2019) collected data from 763 stations and concluded that the UC to the warming trend of T_{mean} was 19.6% during the period 1961–2015. Compared to previous studies, the obtained urbanization impacts on air temperatures in this study is a bit stronger. Different methods, stations, and study periods may contribute to these differences.

4. Conclusions

In this study, daily air temperatures and land-cover data at 30-m spatial resolution and annual temporal resolution from 1985 to 2017 collected at 2454 stations were used to analyze the local urbanization impact on air temperatures. Significant warming trends of T_{max}, T_{min}, T_{mean}, and $T_{(max+min)/2}$ averaged

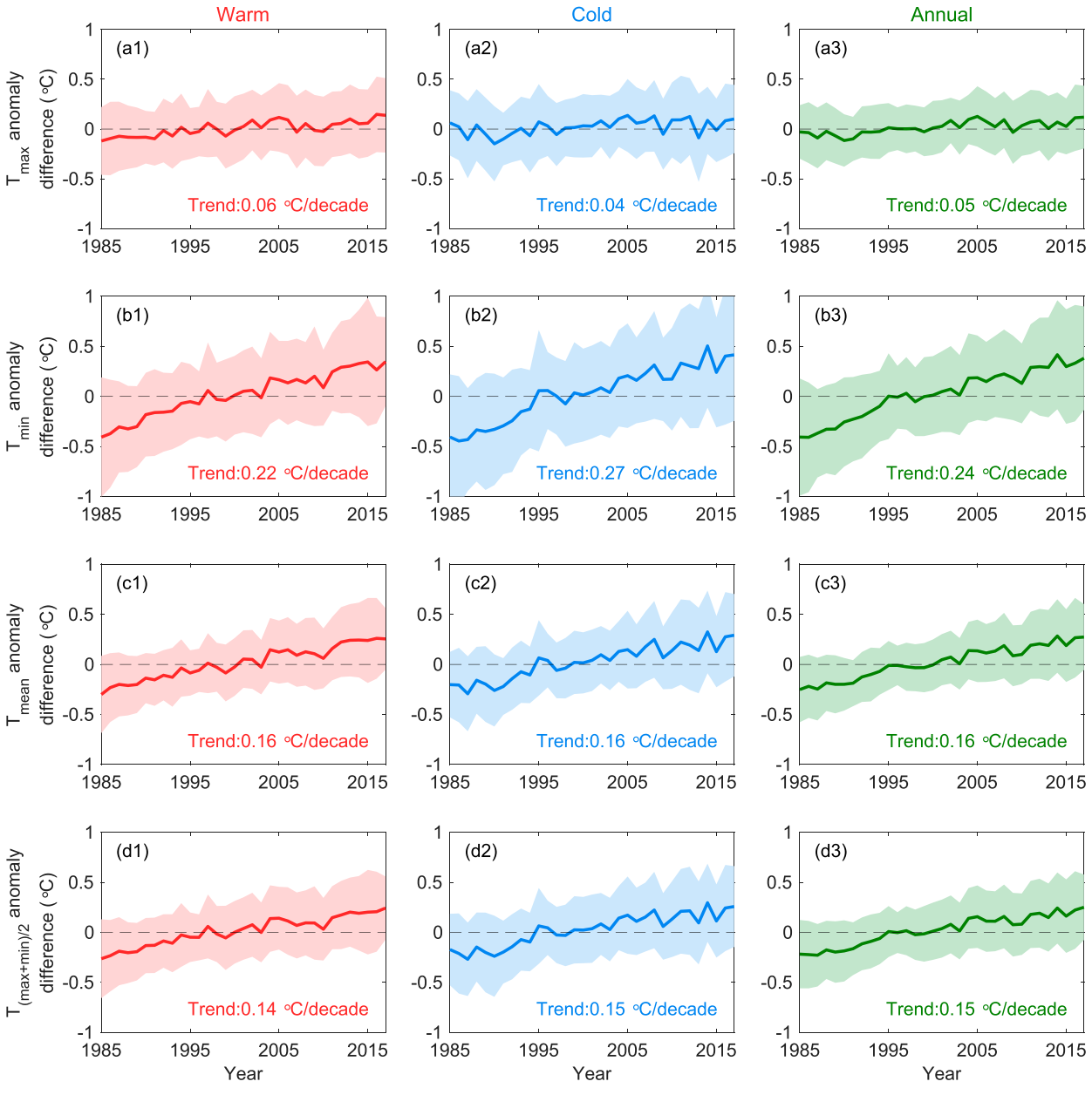

FIG. 11. Time series of urban–rural (a1)–(a3) T_{max}, (b1)–(b3) T_{min}, (c1)–(c3) T_{mean}, and (d1)–(d3) $T_{(max+min)/2}$ anomaly differences averaged from all 242 urban–rural station pairs during warm seasons (May–October), cold seasons (November–April), and the whole year. The shading indicates the standard deviations of T_a anomaly differences among 242 urban–rural station pairs during warm seasons (pink), cold seasons (light blue), and the whole year (light green), which was calculated each year.

from all 2454 stations were observed for warm seasons, cold seasons, and the whole year, with annual warming trends of 0.356°, 0.421°, 0.347°, and 0.388°C decade^{-1}, respectively. A higher warming rate in T_{min} than that in T_{max} was observed during the period 1985–2017, with an annual asymmetry of 0.065°C decade^{-1}, and this asymmetry was also observed during cold seasons (0.054°C decade^{-1}) and warm seasons (0.078°C decade^{-1}). This result was consistent with the findings in previous studies (Liu et al. 2006; Li et al. 2010; Cao et al. 2016).

China has undergone rapid urbanization since the 1978 economic reform (Huang et al. 2017; Yang et al. 2017). Although urbanized areas only occupied 2.25% of the landmass in China in 2017, the local environment around most weather stations has experienced rapid urbanization since 1985. The percentage of stations with an urbanization ratio within 10 km^2 larger than 20% has increased from 22.1% in 1985 to 68.2% in 2017, and the increasing rate of urbanization ratio within 10 km^2 averaged from all 2454 stations has reached

TABLE 2. The average UE (°C decade^{-1}) of, i.e., the urban–rural T_a anomaly difference, and the average UC to the increasing trends in T_{max}, T_{min}, T_{mean}, and $T_{(max+min)/2}$ anomalies at 242 urban–rural station pairs. Warm seasons represent the period from May to October, and cold seasons represent the period from November to April; $T_{(max+min)/2}$ was averaged from T_{max} and T_{min}. A two-tailed t test is employed to test the significance of the UE and UC. Asterisks (*) indicate significance at the $p = 0.01$ confidence level.

	Warm seasons		Cold seasons		The whole year	
T_a anomaly difference	UE	UC	UE	UC	UE	UC
T_{max}	0.062*	17.6%	0.038*	9.5%	0.050*	13.2%
T_{min}	0.220*	39.4%	0.266*	44.9%	0.243*	42.2%
T_{mean}	0.162*	38.9%	0.164*	34.7%	0.163*	36.7%
$T_{(max+min)/2}$	0.141*	30.9%	0.152*	30.6%	0.146*	30.7%

8.02% decade^{-1}. Therefore, the spatial representations of observations at most meteorological stations were affected by the rapid local urbanization.

To better understand the factors driving the observed asymmetric warming rates between T_{min} and T_{max}, the warming trends of air temperatures in urban and rural stations were analyzed separately. Stations with a maximum urbanization ratio below 20% were defined as rural stations, while stations with an urbanization rate higher than 1% yr^{-1} and the highest urbanization ratios higher than 50% were defined as urban stations. The results revealed significant warming trends at both urban and rural stations. The warming trend of T_{min} (0.575°C decade^{-1}) was obviously stronger than that of T_{max} (0.378°C decade^{-1}) in the whole year at urban stations, and this asymmetry at urban stations (0.197°C decade^{-1}) was approximately 3 times larger than the national average asymmetry derived from all 2454 stations (0.065°C decade^{-1}). However, the asymmetry between T_{min} and T_{max} disappeared at rural stations, which was only 0.005°C decade^{-1}.

The local environment around weather stations could significantly impact the observed air temperatures. A significant positive correlation between the urban–rural urbanization ratio difference and the urban–rural T_a anomaly differences was observed. The local urbanization impact on national average T_a derived from all 2454 stations was then evaluated based on this relationship. The local urbanization impact contributed to the national annual warming trend in T_{max}, T_{min}, T_{mean}, and $T_{(max+min)/2}$ by 7.2% (0.026°C decade^{-1}), 30.2% (0.127°C decade^{-1}), 24.4% (0.085°C decade^{-1}), and 19.7% (0.076°C decade^{-1}), respectively. These numbers were slightly different from those reported in previous studies (Ren et al. 2008; Yang et al. 2011; Wang and Ge 2012; Sun et al. 2016); there are a few reasons for the difference in estimates, such as the use of only data with continuous records and the use of data with no relocation records.

In summary, this study provides insights into explaining the observed asymmetric warming rates between T_{min} and T_{max} in the evaluation of the local urbanization impact on air temperatures. The warming rates in air temperatures are generally evaluated based on meteorological observations, which are closely related to the environmental change around the stations. The superiority of the method is that the latest released high-resolution land-cover data were used, which can describe the observational environment more directly and reliably than most previous studies. Notably, the results show that environments around most stations in China have experienced rapid local urbanization, hence the spatial representations of observations at most stations were affected. Therefore, the meteorological observations show a combined result of large-scale climate changes and local urbanization impact. That is why the asymmetric warming rates between T_{min} and T_{max} are obvious at urbanized stations and still exist in the national average warming rates but disappeared at rural stations. This study also has a meaningful implication for the argument of whether the urbanization impact on warming trends in China is large, small, or even negligible (Li et al. 2010; F. Wang et al. 2015; Z. Yan et al. 2016; J. Wang et al. 2017; Li et al. 2019; Scafetta and Ouyang 2019). In other words, the asymmetric warming rates and the urbanization impact on them may be much smaller in most nonurbanized areas of China if the spatial representation of most stations has not been greatly impacted.

There are still some limitations in this study that may bring some bias in quantifying the local urbanization impact on

TABLE 3. As in Table 2, but derived from 87 single urban–rural station pairs instead of 242 urban–rural station pairs. Asterisks (*) indicate significance at the $p = 0.01$ confidence level.

	Warm seasons		Cold seasons		The whole year	
T_a anomaly difference	UE	UC	UE	UC	UE	UC
T_{max}	0.055*	13.9%	0.032*	8.1%	0.043*	11.0%
T_{min}	0.203*	36.1%	0.226*	39.2%	0.214*	37.7%
T_{mean}	0.15*	34.5%	0.143*	30.8%	0.146*	32.6%
$T_{(max+min)/2}$	0.129*	26.9%	0.129*	26.5%	0.129*	26.7%

TABLE 4. The national average UE (°C decade^{-1}) of and the national average UC to the observed warming rate at all 2454 stations. They were calculated using a polynomial fit based on the national average urbanization ratio and the relationship between the urban–rural urbanization ratio difference and T_a anomaly differences. Warm seasons represent the period from May to October, and cold seasons represent the period from November to April; $T_{(max+min)/2}$ was averaged from T_{max} and T_{min}. A two-tailed t test is employed to test the significance of the UE and UC. Asterisks (*) indicate significance at the $p = 0.01$ confidence level.

	Warm seasons		Cold seasons		The whole year	
T_a anomaly difference	UE	UC	UE	UC	UE	UC
T_{max}	0.032*	9.6%	0.019*	5.1%	0.026*	7.2%
T_{min}	0.115*	27.8%	0.139*	32.5%	0.127*	30.2%
T_{mean}	0.084*	25.9%	0.085*	23.1%	0.085*	24.4%
$T_{(max+min)/2}$	0.074*	19.6%	0.079*	19.7%	0.076*	19.7%

observed warming rates based on observations at all 2454 stations. First, the distribution of the stations is uneven and generally set up according to the distribution of counties in China. Second, due to the data inhomogeneity caused by station relocations, only the longest continuous record without relocations at each station was used to analyze local urbanization impacts on air temperatures. Third, the detailed description of changes in the surrounding of stations is still lacking. Last but not least, other factors, such as the effect of greenhouse gases, were not considered in this study. These limitations should be gradually improved in future studies.

Acknowledgments. This study was sponsored by the National Key R&D Program of China (2017YFA0603601), the National Natural Science Foundation of China (41525018 and 41930970), and the K.C. Wong Magna Fund in Ningbo University. The meteorological observations were obtained from the Chinese Meteorological Information Center (http://data.cma.cn/data/cdcdetail/dataCode/SURF_CLI_CHN_MUL_DAY_V3.0.html). The land-cover type data at 30-m resolution were obtained from the National Geomatics Center of China (http://data.ess.tsinghua.edu.cn/urbanRuralChina.html).

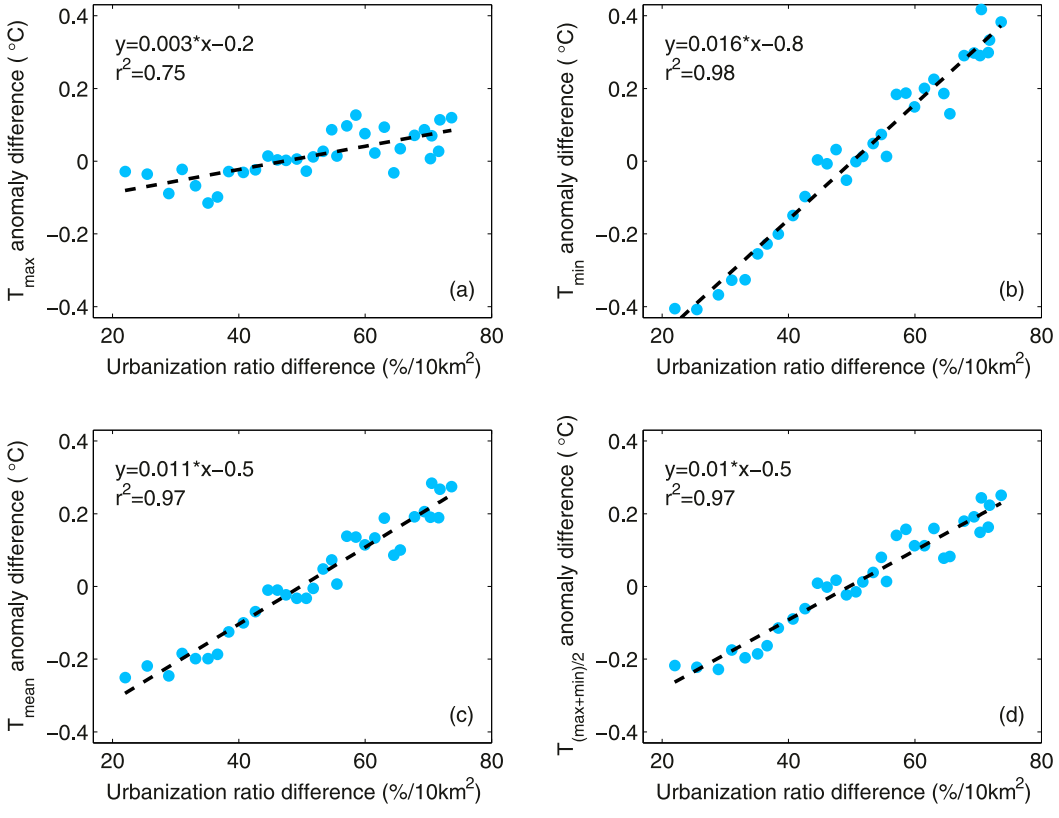

FIG. 12. Scatterplots of mean urban–rural urbanization ratio differences at 242 urban–rural station pairs as a function of annual urban–rural (a) T_{max}, (b) T_{min}, (c) T_{mean}, and (d) $T_{(max+min)/2}$ anomaly difference.

REFERENCES

Akbari, H., and Coauthors, 2015: Local climate change and urban heat island mitigation techniques—The state of the art. *J. Civil Eng. Manage.*, **22** (1), 1–16, https://doi.org/10.3846/13923730.2015.1111934.

Arguez, A., and R. S. Vose, 2011: The definition of the standard WMO climate normal: The key to deriving alternative climate normals. *Bull. Amer. Meteor. Soc.*, **92**, 699–704, https://doi.org/10.1175/2010BAMS2955.1.

Bernhardt, J., and A. M. Carleton, 2019: Comparing daily temperature averaging methods: The role of surface and atmosphere variables in determining spatial and seasonal variability. *Theor. Appl. Climatol.*, **136**, 499–512, https://doi.org/10.1007/s00704-018-2504-7.

——, ——, and C. LaMagna, 2018: A comparison of daily temperature-averaging methods: Spatial variability and recent change for the CONUS. *J. Climate*, **31**, 979–996, https://doi.org/10.1175/JCLI-D-17-0089.1.

Bian, T., and G. Ren, 2017: Reassessment of urbanization effect on surface air temperature trends at an urban station of North China. *Meteor. Atmos. Phys.*, **131**, 237–250, https://doi.org/10.1007/s00703-017-0568-z.

——, and ——, 2019: Reassessment of urbanization effect on surface air temperature trends at an urban station of North China. *Meteor. Atmos. Phys.*, **131**, 237–250, https://doi.org/10.1007/s00703-017-0568-z.

Cao, L., Y. Zhu, G. Tang, F. Yuan, and Z. Yan, 2016: Climatic warming in China according to a homogenized data set from 2419 stations. *Int. J. Climatol.*, **36**, 4384–4392, https://doi.org/10.1002/joc.4639.

Chrysanthou, A., G. van der Schrier, E. J. M. van den Besselaar, A. M. G. Klein Tank, and T. Brandsma, 2014: The effects of urbanization on the rise of the European temperature since 1960. *Geophys. Res. Lett.*, **41**, 7716–7722, https://doi.org/10.1002/2014GL061154.

Dou, Y., B. Qu, Y. Tao, and S. Hu, 2008: The application of quality control procedures for real-time data from automatic weather stations. *Meteor. Mon.*, **34**, 77–81.

Du, J., K. Wang, J. Wang, and Q. Ma, 2017: Contributions of surface solar radiation and precipitation to the spatiotemporal patterns of surface and air warming in China from 1960 to 2003. *Atmos. Chem. Phys.*, **17**, 4931–4944, https://doi.org/10.5194/acp-17-4931-2017.

Easterling, D. R., and Coauthors, 1997: Maximum and minimum temperature trends for the globe. *Science*, **277**, 364–367, https://doi.org/10.1126/science.277.5324.364.

Founda, D., and M. Santamouris, 2017: Synergies between urban heat island and heat waves in Athens (Greece), during an extremely hot summer (2012). *Sci. Rep.*, **7**, 10973, https://doi.org/10.1038/s41598-017-11407-6.

Gilgen, H., M. Wild, and A. Ohmura, 1998: Means and trends of shortwave irradiance at the surface estimated from global energy balance archive data. *J. Climate*, **11**, 2042–2061, https://doi.org/10.1175/1520-0442-11.8.2042.

Gong, P., X. Li, and W. Zhang, 2019a: 40-year (1978–2017) human settlement changes in China reflected by impervious surfaces from satellite remote sensing. *Sci. Bull.*, **64**, 756–763, https://doi.org/10.1016/j.scib.2019.04.024.

——, and Coauthors, 2019b: Stable classification with limited sample: Transferring a 30-m resolution sample set collected in 2015 to mapping 10-m resolution global land cover in 2017. *Sci. Bull.*, **64**, 370–373, https://doi.org/10.1016/j.scib.2019.03.002.

Grimmond, S., 2007: Urbanization and global environmental change: Local effects of urban warming. *Geogr. J.*, **173**, 83–88, https://doi.org/10.1111/j.1475-4959.2007.232_3.x.

Hansen, J., and S. Lebedeff, 1987: Global trends of measured surface air temperature. *J. Geophys. Res.*, **92**, 13 345–13 372, https://doi.org/10.1029/JD092iD11p13345.

Hausfather, Z., M. J. Menne, C. N. Williams, T. Masters, R. Broberg, and D. Jones, 2013: Quantifying the effect of urbanization on U.S. Historical Climatology Network temperature records. *J. Geophys. Res. Atmos.*, **118**, 481–494, https://doi.org/10.1029/2012JD018509.

He, Y., K. Wang, C. Zhou, and M. Wild, 2018: A revisit of global dimming and brightening based on the sunshine duration. *Geophys. Res. Lett.*, **45**, 4281–4289, https://doi.org/10.1029/2018GL077424.

Hoegh-Guldberg, O., and Coauthors, 2018: Impacts of 1.5°C global warming on natural and human systems. *Global Warming of 1.5°C*, V. Masson-Delmotte et al., Eds., Cambridge University Press, 175–311, https://www.ipcc.ch/site/assets/uploads/sites/2/2019/06/SR15_Chapter3_Low_Res.pdf.

Hua, L., Z. Ma, and W. Guo, 2008: The impact of urbanization on air temperature across China. *Theor. Appl. Climatol.*, **93**, 179–194, https://doi.org/10.1007/s00704-007-0339-8.

Huang, H. B., and Coauthors, 2017: Mapping major land cover dynamics in Beijing using all Landsat images in Google Earth Engine. *Remote Sens. Environ.*, **202**, 166–176, https://doi.org/10.1016/j.rse.2017.02.021.

Jiang, S., and K. Wang, 2018: Exploring the holiday effect on air temperatures. *Sci. Rep.*, **8**, 17943, https://doi.org/10.1038/s41598-018-36351-x.

——, X. Lee, J. Wang, and K. Wang, 2019: Amplified urban heat islands during heat wave periods. *J. Geophys. Res. Atmos.*, **124**, 7797–7812, https://doi.org/10.1029/2018JD030230.

Kaloustian, N., and Y. Diab, 2015: Effects of urbanization on the urban heat island in Beirut. *Urban Climate*, **14**, 154–165, https://doi.org/10.1016/j.uclim.2015.06.004.

Lazzarini, M., P. R. Marpu, and H. Ghedira, 2013: Temperature-land cover interactions: The inversion of urban heat island phenomenon in desert city areas. *Remote Sens. Environ.*, **130**, 136–152, https://doi.org/10.1016/j.rse.2012.11.007.

Li, D., E. Bou-Zeid, and M. Oppenheimer, 2014: The effectiveness of cool and green roofs as urban heat island mitigation strategies. *Environ. Res. Lett.*, **9**, 055002, https://doi.org/10.1088/1748-9326/9/5/055002.

Li, Q., W. Li, P. Si, X. Gao, W. Dong, P. Jones, J. Huang, and L. Cao, 2010: Assessment of surface air warming in northeast China, with emphasis on the impacts of urbanization. *Theor. Appl. Climatol.*, **99**, 469–478, https://doi.org/10.1007/s00704-009-0155-4.

Li, X., and P. Gong, 2016: An "exclusion-inclusion" framework for extracting human settlements in rapidly developing regions of China from Landsat images. *Remote Sens. Environ.*, **186**, 286–296, https://doi.org/10.1016/j.rse.2016.08.029.

——, ——, and L. Liang, 2015: A 30-year (1984–2013) record of annual urban dynamics of Beijing City derived from Landsat data. *Remote Sens. Environ.*, **166**, 78–90, https://doi.org/10.1016/j.rse.2015.06.007.

——, Y. Zhou, G. R. Asrar, M. Imhoff, and X. Li, 2017: The surface urban heat island response to urban expansion: A panel analysis for the conterminous United States. *Sci. Total Environ.*, **605–606**, 426–435, https://doi.org/10.1016/j.scitotenv.2017.06.229.

Li, Y., L. Wang, H. Zhou, G. Zhao, F. Ling, X. Li, and J. Qiu, 2019: Urbanization effects on changes in the observed air temperatures

during 1977–2014 in China. *Int. J. Climatol.*, **39**, 251–265, https://doi.org/10.1002/joc.5802.

Li, Z., and Z. Yan, 2009: Homogenized daily mean/maximum/minimum temperature series for China from 1960-2008. *Atmos. Oceanic Sci. Lett.*, **2**, 237–243, https://doi.org/10.1080/16742834.2009.11446802.

——, K. Wang, C. Zhou, and L. Wang, 2016: Modelling the true monthly mean temperature from continuous measurements over global land. *Int. J. Climatol.*, **36**, 2103–2110, https://doi.org/10.1002/joc.4445.

Lin, J., and Q. Zhang, 2015: Characteristics of China climate states change and its impact on the analysis of climate change. *Plateau Meteor.*, **34**, 1593–1600.

Liu, X., Z. Yin, X. Shao, and N. Qin, 2006: Temporal trends and variability of daily maximum and minimum, extreme temperature events, and growing season length over the eastern and central Tibetan Plateau during 1961–2003. *J. Geophys. Res.*, **111**, D19109, https://doi.org/10.1029/2005JD006915.

Liu, Y., G. Ren, H. Kang, and X. Sun, 2019: A significant bias of Tmax and Tmin average temperature and its trend. *J. Appl. Meteor. Climatol.*, **58**, 2235–2246, https://doi.org/10.1175/JAMC-D-19-0001.1.

Liu, Z., C. He, Q. Zhang, Q. Huang, and Y. Yang, 2012: Extracting the dynamics of urban expansion in China using DMSP-OLS nighttime light data from 1992 to 2008. *Landsc. Urban Plann.*, **106**, 62–72, https://doi.org/10.1016/j.landurbplan.2012.02.013.

Miao, S., J. Dou, F. Chen, J. Li, and A. Li, 2012: Analysis of observations on the urban surface energy balance in Beijing. *Sci. China Earth Sci.*, **55**, 1881–1890, https://doi.org/10.1007/s11430-012-4411-6.

Muller, C. L., L. Chapman, C. S. B. Grimmond, D. T. Young, and X.-M. Cai, 2013: Toward a standardized metadata protocol for urban meteorological networks. *Bull. Amer. Meteor. Soc.*, **94**, 1161–1185, https://doi.org/10.1175/BAMS-D-12-00096.1.

Oke, T. R., 1973: City size and the urban heat island. *Atmos. Environ.*, **7**, 769–779, https://doi.org/10.1016/0004-6981(73)90140-6.

——, 1976: The distinction between canopy and boundary-layer urban heat islands. *Atmosphere*, **14**, 268–277, https://doi.org/10.1080/00046973.1976.9648422.

——, 1982: The energetic basis of the urban heat island. *Quart. J. Roy. Meteor. Soc.*, **108**, 1–24, https://doi.org/10.1002/QJ.49710845502.

Parker, D. E., 2006: A demonstration that large-scale warming is not urban. *J. Climate*, **19**, 2882–2895, https://doi.org/10.1175/JCLI3730.1.

Peng, S., and Coauthors, 2013: Asymmetric effects of daytime and night-time warming on Northern Hemisphere vegetation. *Nature*, **501**, 88–92, https://doi.org/10.1038/nature12434.

Pepin, N., and Coauthors, 2015: Elevation-dependent warming in mountain regions of the world. *Nat. Climate Change*, **5**, 424–430, https://doi.org/10.1038/nclimate2563.

Ren, G., and Y. Zhou, 2014: Urbanization effect on trends of extreme temperature indices of national stations over mainland China, 1961–2008. *J. Climate*, **27**, 2340–2360, https://doi.org/10.1175/JCLI-D-13-00393.1.

——, ——, Z. Chu, J. Zhou, A. Zhang, J. Guo, and X. Liu, 2008: Urbanization effects on observed surface air temperature trends in North China. *J. Climate*, **21**, 1333–1348, https://doi.org/10.1175/2007JCLI1348.1.

Ren, Y., and G. Ren, 2011: A remote-sensing method of selecting reference stations for evaluating urbanization effect on surface air temperature trends. *J. Climate*, **24**, 3179–3189, https://doi.org/10.1175/2010JCLI3658.1.

Rinner, C., and M. Hussain, 2011: Toronto's urban heat island—Exploring the relationship between land use and surface temperature. *Remote Sens.*, **3**, 1251–1265, https://doi.org/10.3390/rs3061251.

Scafetta, N., and S. Ouyang, 2019: Detection of UHI bias in China climate network using Tmin and Tmax surface temperature divergence. *Global Planet. Change*, **181**, 102989, https://doi.org/10.1016/j.gloplacha.2019.102989.

Shi, Z., G. Jia, Y. Hu, and Y. Zhou, 2019: The contribution of intensified urbanization effects on surface warming trends in China. *Theor. Appl. Climatol.*, **138**, 1125–1137, https://doi.org/10.1007/s00704-019-02892-y.

Singh, P., N. Kikon, and P. Verma, 2017: Impact of land use change and urbanization on urban heat island in Lucknow city, central India. A remote sensing based estimate. *Sustainable Cities Soc.*, **32**, 100–114, https://doi.org/10.1016/j.scs.2017.02.018.

Stewart, I. D., and T. R. Oke, 2012: Local climate zones for urban temperature studies. *Bull. Amer. Meteor. Soc.*, **93**, 1879–1900, https://doi.org/10.1175/BAMS-D-11-00019.1.

Sun, Y., X. Zhang, G. Ren, F. W. Zwiers, and T. Hu, 2016: Contribution of urbanization to warming in China. *Nat. Climate Change*, **6**, 706–709, https://doi.org/10.1038/nclimate2956.

——, T. Hu, X. Zhang, C. Li, C. Lu, G. Ren, and Z. Jiang, 2019: Contribution of global warming and urbanization to changes in temperature extremes in eastern China. *Geophys. Res. Lett.*, **46**, 11 426–11 434, https://doi.org/10.1029/2019GL084281.

Sutton, R. T., B. Dong, and J. M. Gregory, 2007: Land/sea warming ratio in response to climate change: IPCC AR4 model results and comparison with observations. *Geophys. Res. Lett.*, **34**, L02701, https://doi.org/10.1029/2006GL028164.

Tang, H., and P. Zhai, 2005: Comparison of variations of surface air temperatures in eastern and western China during 1951~2002. *Chin. J. Geophys.*, **48**, 526–534, https://doi.org/10.1002/cjg2.691.

Torres-Alavez, A., T. Cavazos, and C. Turrent, 2014: Land–sea thermal contrast and intensity of the North American monsoon under climate change conditions. *J. Climate*, **27**, 4566–4580, https://doi.org/10.1175/JCLI-D-13-00557.1.

Tysa, S. K., G. Ren, Y. Qin, P. Zhang, Y. Ren, W. Jia, and K. Wen, 2019: Urbanization effect in regional temperature series based on a remote sensing classification scheme of stations. *J. Geophys. Res.*, **124**, 10 646–10 661, https://doi.org/10.1029/2019JD030948.

Vose, R. S., T. R. Karl, D. R. Easterling, C. N. Williams, and M. J. Menne, 2004: Impact of land-use change on climate. *Nature*, **427**, 213–214, https://doi.org/10.1038/427213b.

Wang, F., and Q. Ge, 2012: Estimation of urbanization bias in observed surface temperature change in China from 1980 to 2009 using satellite land-use data. *Chin. Sci. Bull.*, **57**, 1708–1715, https://doi.org/10.1007/s11434-012-4999-0.

——, ——, S. Wang, Q. Li, and P. D. Jones, 2015: A new estimation of urbanization's contribution to the warming trend in China. *J. Climate*, **28**, 8923–8938, https://doi.org/10.1175/JCLI-D-14-00427.1.

Wang, J., Z. Yan, Z. Li, W. Liu, and Y. Wang, 2013: Impact of urbanization on changes in temperature extremes in Beijing during 1978–2008. *Chin. Sci. Bull.*, **58**, 4679–4686, https://doi.org/10.1007/s11434-013-5976-y.

——, S. F. B. Tett, and Z. Yan, 2017: Correcting urban bias in large-scale temperature records in China, 1980–2009. *Geophys. Res. Lett.*, **44**, 401–408, https://doi.org/10.1002/2016GL071524.

Wang, K., 2014: Sampling biases in datasets of historical mean air temperature over land. *Sci. Rep.*, **4**, 4637, https://doi.org/10.1038/srep04637.

——, Q. Ma, Z. Li, and J. Wang, 2015: Decadal variability of surface incident solar radiation over China: Observations, satellite retrievals, and reanalyses. *J. Geophys. Res. Atmos.*, **120**, 6500–6514, https://doi.org/10.1002/2015JD023420.

——, Y. Li, Y. Wang, and X. Yang, 2017: On the asymmetry of the urban daily air temperature cycle. *J. Geophys. Res. Atmos.*, **122**, 5625–5635, https://doi.org/10.1002/2017JD026589.

——, S. Jiang, J. Wang, C. Zhou, X. Wang, and X. Lee, 2017: Comparing the diurnal and seasonal variabilities of atmospheric and surface urban heat islands based on the Beijing urban meteorological network. *J. Geophys. Res. Atmos.*, **122**, 2131–2154, https://doi.org/10.1002/2016JD025304.

Wen, K., G. Ren, J. Li, A. Zhang, Y. Ren, X. Sun, and Y. Zhou, 2019: Recent surface air temperature change over mainland China based on an urbanization-bias adjusted dataset. *J. Climate*, **32**, 2691–2705, https://doi.org/10.1175/JCLI-D-18-0395.1.

World Meteorological Organization, 2011: Guide to climatological practices. WMO Rep. 100, 117 pp.

Xu, X., J. E. González, S. Shen, S. Miao, and J. Dou, 2018: Impacts of urbanization and air pollution on building energy demands—Beijing case study. *Appl. Energy*, **225**, 98–109, https://doi.org/10.1016/j.apenergy.2018.04.120.

Yan, L., Z. Liu, G. Chen, J. E. Kutzbach, and X. Liu, 2016: Mechanisms of elevation-dependent warming over the Tibetan Plateau in quadrupled CO_2 experiments. *Climatic Change*, **135**, 509–519, https://doi.org/10.1007/s10584-016-1599-z.

Yan, Z., J. Wang, J. Xia, and J. Feng, 2016: Review of recent studies of the climatic effects of urbanization in China. *Adv. Climate Change Res.*, **7**, 154–168, https://doi.org/10.1016/j.accre.2016.09.003.

Yang, J., T. Wu, and G. Peng, 2017: Implementation of China's new urbanization strategy requires new thinking. *Sci. Bull.*, **62**, 81–82, https://doi.org/10.1016/j.scib.2016.12.013.

Yang, X., Y. Hou, and B. Chen, 2011: Observed surface warming induced by urbanization in east China. *J. Geophys. Res.*, **116**, D14113, https://doi.org/10.1029/2010JD015452.

You, Q., S. Kang, N. Pepin, and Y. Yan, 2008: Relationship between trends in temperature extremes and elevation in the eastern and central Tibetan Plateau, 1961–2005. *Geophys. Res. Lett.*, **35**, L04704, https://doi.org/10.1029/2007GL032669.

Zhang, A., G. Ren, J. Zhou, Z. Chu, Y. Ren, and G. Tang, 2010: Urbanization effect on surface air temperature trends over China. *Acta Meteor. Sin.*, **68**, 957–966.

Zhao, L., X. Lee, R. B. Smith, and K. Oleson, 2014: Strong contributions of local background climate to urban heat islands. *Nature*, **511**, 216–219, https://doi.org/10.1038/nature13462.

Zheng, Z., and Coauthors, 2018: Relationship between fine-particle pollution and the urban heat island in Beijing, China: Observational evidence. *Bound.-Layer Meteor.*, **169**, 93–113, https://doi.org/10.1007/s10546-018-0362-6.

Zhou, L., R. E. Dickinson, Y. Tian, J. Fang, Q. Li, R. K. Kaufmann, C. J. Tucker, and R. B. Myneni, 2004: Evidence for a significant urbanization effect on climate in China. *Proc. Natl. Acad. Sci. USA*, **101**, 9540–9544, https://doi.org/10.1073/pnas.0400357101.